Indian Journal of Chemical Technology
Vol. 33, March 2026, pp. 217-227
DOI: 10.56042/ijct.v33i2.22185

Sustainable removal of metanil yellow from aqueous systems via adsorption on *Jatropha* biodiesel cake nanobiomaterial

Dhruva Vyas[1], Manali Rathod[1], Yasmin Khambhaty[2]* & Shaik Basha[1,3]

[1]Marine Biotechnology and Ecology Division, CSIR-Central Salt & Marine Chemicals Research Institute, Bhavnagar 364 002, Gujarat, India

[2]Environmental Science Lab, CSIR-Central Leather Research Institute, Adyar, Chennai, 600 020, Tamil Nadu, India

[3]Hyderabad Zonal Centre, CSIR-National Environmental Engineering Research Institute, IICT Campus, Tarnaka, Hyderabad 500007, India

*E-mail: yasmink.clri@csir.res.in

Received 30 July 2025; accepted 13 February 2026

The biosorption behaviour of metanil yellow from aqueous solution has been investigated in a batch system using a low-cost biochar-based nanobiomaterial prepared from *Jatropha* oil cake (JOC). The optimum pH was 4.0, which provided a maximum biosorption capacity of 21.71 mg/g and the equilibrium was established in 90 min. Kinetic analysis indicated that the contribution of intraparticle diffusion increased with dye concentration, whereas the apparent influence of film and pore diffusion decreased. Equilibrium data was well represented by the Sips isotherm followed by the Langmuir model, which confirmed monolayer coverage with maximum sorption capacity of 24.3 mg/g. Transmission Electron Microscopy (TEM) revealed primary particles in the nanoscale range (≈60–80 nm), which exhibited partial aggregation. Fourier Transform Infrared Spectrometer (FTIR) analysis suggested the involvement of ion-exchange and surface complexation during the biosorption process. Desorption studies showed that up to 96.3% of metanil yellow could be recovered from the biochar using acetone. The results demonstrated that the nanobiomaterial derived from *Jatropha* biodiesel cake could be leveraged as a low-cost adsorbent for the removal of dye from the water environment.

Keywords: Adsorption, Isotherm, Kinetics, Metanil yellow, Nanosorbent

Introduction

Globally, synthetic dyes are extensively used in industries such as textiles, leather, pulp and paper, printing, and cosmetics[1]. A considerable fraction of dye-containing effluents is discharged into water bodies with inadequate or no treatment, resulting in reduced light penetration, disruption of photosynthetic activity, and adverse impacts on aquatic ecosystems[2]. In addition to aesthetic concerns, many dyes exhibit toxic, mutagenic, or carcinogenic properties, making their effective removal from wastewater an important environmental challenge[3,4,5,6].

Metanil Yellow (3-(4-anilinophenylazo) benzene sulfonic acid sodium salt) is an anionic acidic azo dye widely used in textile, leather, paper, soap, and pigment applications but is a non-permitted food colorant with reported carcinogenic effects[7]. Exposure to metanil yellow has been associated with adverse biological effects, including tumor promotion, reproductive toxicity, and physiological alterations in aquatic organisms[7,8]. Even at low concentrations, its presence in wastewater limits water reuse potential and poses risks to aquatic ecosystems and human health. Among the various physicochemical treatment methods available for dye-laden wastewater, adsorption is regarded as one of the most effective and economically feasible approaches[9]. In recent years, increasing attention has been given to biomass-derived adsorbents owing to their low cost, availability, and lower environmental footprint compared to conventional synthetic materials[10].

Jatropha oil cake (JOC), a solid by-product generated during biodiesel production from *Jatropha curcas* seeds, represents an abundant agro-industrial residue with limited disposal options. Previous studies have reported its applicability as a biosorbent for the removal of contaminants such as heavy metals and ammoniacal nitrogen[11,12]. The lignocellulosic composition and surface functional groups present in JOC make it a suitable precursor for adsorbent materials, while its utilization contributes to waste valorization and sustainable resource management. Although adsorption of metanil yellow using biomass- and biochar-derived materials has been widely explored, the present study differs in the design and functional scale of the adsorbent. Unlike

conventional *Jatropha*-based agro-waste or biochar materials that primarily rely on bulk porosity and surface heterogeneity, the prepared nanobiomaterial exhibits a nanostructured architecture that enhances surface accessibility and shortens effective intraparticle diffusion pathways. This structural feature contributes to faster initial uptake and distinct mass-transfer behaviour. Accordingly, this work emphasizes how nanoscale structuring of a biogenic material influences adsorption kinetics and transport characteristics, rather than focusing solely on adsorption capacity or extensive model fitting.

In this study, biochar derived from JOC was evaluated for the adsorption of metanil yellow from aqueous solutions. The effects of solution pH, adsorbent dosage, contact time, and initial dye concentration were investigated through batch experiments. Adsorption kinetics, equilibrium isotherms, and desorption behaviour were examined to assess adsorption performance and to examine the interaction behaviour between metanil yellow and the *Jatropha* oil cake-derived material.

Experimental Section

Materials

All reagents used in this study were of analytical grade and employed without any further purification. Metanil Yellow (molecular formula: $C_{18}H_{14}N_3NaO_3S$; C.I. No. 13065; CAS No. 587-98-4; molecular weight: 375.38), along with nitric acid (HNO_3) and sodium hydroxide (NaOH), were procured from Merck, India.

Preparation of the nanosorbent, biochar

Jatropha curcas L. press-cake, obtained from the biodiesel plant of CSIR-CSMCRI, was thoroughly washed with tap water to eliminate physical impurities and dried overnight in an oven at 120°C. The dried biomass was treated with a KOH solution and subjected to a two-step thermal process: initial heating at 120°C for 2 h, followed by pyrolysis in a muffle furnace at 500°C for 4 h. The resulting biochar was allowed to cool to room temperature, ground into a fine powder, stored in a glass bottle, and used for subsequent experiments.

Biosorption /Desorption studies

All experiments, except for those assessing temperature effects, were conducted at a constant temperature of 25 ± 2 °C. Batch equilibrium biosorption studies were performed in 50 mL Erlenmeyer flasks containing 25 mL of metanil yellow solutions (5–100 mg/L). A fixed amount of nanosorbent (50 mg) was added to each flask, and agitated on a rotary shaker. Solution pH was adjusted using HNO_3 or NaOH. After 6 h of shaking, samples were filtered through a 0.45 µm Millipore membrane, and the dye concentration was measured at 438 nm using a Shimadzu UV-Vis spectrophotometer. The effect of pH was studied over a pH range of 2–11 using 50 mg/L dye solutions. Kinetic experiments were carried out using 250 mL solutions added with 500 mg of nanosorbent, agitated at 140 rpm, with samples taken at pre-set intervals for analysis.

To evaluate reusability, desorption studies were conducted using EDTA, acetic acid, HCl, acetone, and water. Dye-loaded nanosorbent (prepared using 10 mg/L dye solution) was separated by centrifugation, mixed with 5% desorbing agents, and shaken for 3 h at 140 rpm. The mixtures were filtered, and dye concentrations in the supernatant were analyzed. Control tests confirmed negligible dye adsorption on flask walls or filter membranes in the absence of nanosorbent. All experiments were performed in duplicate and demonstrated good reproducibility, with only minor variation between repeated measurements.

Characterization of nanosorbent

The morphology of the nanosorbent was analyzed using TEM, JEOL JEM-2100 operated at an acceleration voltage of 200 keV, and atomic force microscopy (AFM, NT-MDT NTEGRA, TS 150, Russia), with image processing carried out using Nova Px software (version 3.2.5 12501).

FTIR spectra of both raw and metanil yellow-loaded nanosorbents were recorded using a Perkin-Elmer GX 2000 spectrometer. Approximately 30 mg of nanosorbent was mixed with 300 mg of KBr (Sigma) and pressed into translucent pellets. The spectra were collected over the range of 400–4000 cm^{-1}, with 10 scans at a resolution of 4 cm^{-1}.

Dye uptake capacity

The dye uptake at equilibrium, q_e (mg/g) was calculated from the difference in dye concentration before and after biosorption, as per Eq. (1):

$$q_e = \frac{V(C_i - C_e)}{W} \quad \ldots (1)$$

Here, V represents the volume of the dye solution (L), C_1 and C_e are the initial and equilibrium dye concentrations in the solution (mg/L), respectively, and W denotes the mass of the nanosorbent (g). All model parameters were determined using non-linear regression analysis performed with DATAFIT® software (Oakdale Engineering, USA).

Results and Discussion

Effect of initial pH

pH plays a critical role in controlling the adsorption capacity of nanosorbents. The effect of initial pH (2–11) on the adsorption of metanil yellow (50 mg/L) exhibited an increased sorption capacity from 13.35 to 21.71 mg/g as pH rose from 2 to 4, beyond that the adsorption capacity of the nanosorbent was not significantly affected (Fig. 1). This behaviour can be attributed to changes in solution pH, which influence the surface charge of the adsorbent. The azoic dye produces negatively charged ions when dissolved in water. The reported pH_{pzc} values for biochar was 8.2[13]. At pH values lower than the corresponding pH_{pzc} value, the biochar will have a net positive charge. Thus, the nanosorbent favours the adsorption of the anionic dye owing to increasing electrostatic attractions between the positively charged functional groups located on the surface of the nanosorbent and the negatively charged dye anions. At pH values higher than the corresponding pH_{pzc}, the surface of nanosorbent tends to acquire negative charge, resulting in the decreased adsorption of metanil yellow[14]. Similar results were obtained for metanil yellow adsorption onto fly ash[15] and chemically cross-linked chitosan beads[16]. The adsorption capacity showed limited sensitivity to solution pH, indicating potential suitability for practical wastewater treatment applications.

Biosorption kinetics

Fig. 2 illustrates the influence of contact time on the sorption capacity of the nanosorbent at varying initial concentrations of metanil yellow. Rapid dye uptake occurred within the first 10 min, followed by a slower phase, with equilibrium within 90 min. Over 85% of the dye was adsorbed within 30 min. This fast-initial uptake is attributed to abundant active sites and a steep concentration gradient between the dye in solution and on the nanosorbent surface. Once the sites were occupied, the rate get slowed[17]. The rapid adsorption kinetics suggests that the nanosorbent may be suitable for application in continuous-flow water treatment systems.

Kinetic studies suggested that the biosorption process followed diffusion through a boundary layer, likely making it the rate-limiting step[18]. The values for equilibrium biosorption capacity as predicted by the pseudo-first order model was very low (3.15-6.26 mg/g) as compared to experimental values (7.12-10.75 mg/g) although theregression coefficients (R^2) ranged from 0.857 to 0.884 (Table 1). The predicted kinetics showed that the pattern for the dye uptake as described by the pseudo-first order model was analogous to various initial concentrations. Although the pseudo-first order model fit the initial phase (R^2 = 0.857–0.884), it underestimated

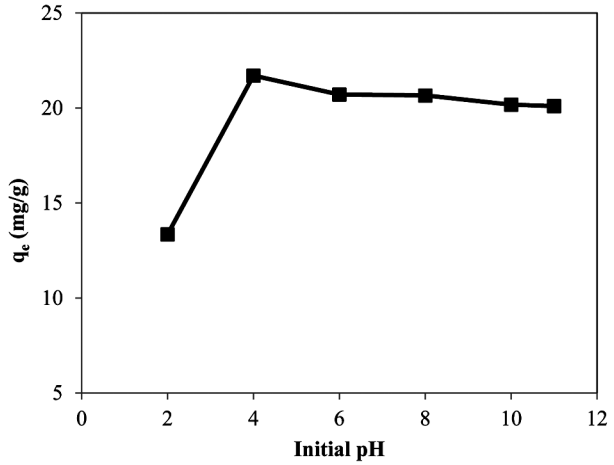

Fig. 1 — Effect of initial pH on sorption of metanil yellow onto nanosorbent (initial dye concentration: 50 mg/L, biosorbent dose: 2.0 g/L, temperature: 25°C, agitating rate: 140 rpm)

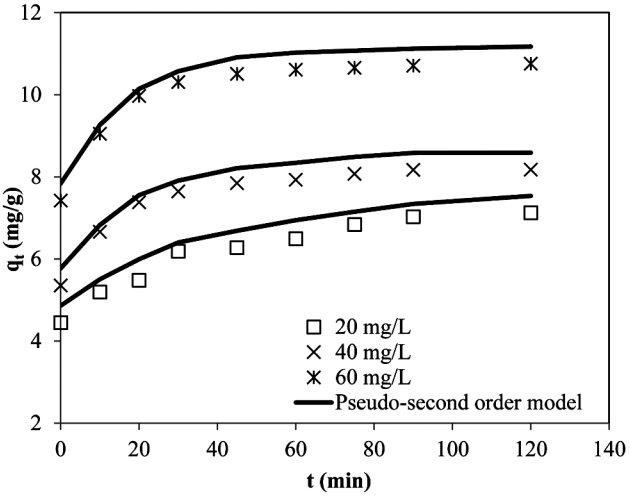

Fig. 2 — The pseudo-second-order kinetics for the sorption of metanil yellow onto nanosorbent (pH: 4.0, biosorbent dose: 2.0 g/L, temperature: 25°C, agitating rate: 140 rpm)

Table 1 — Parameters of kinetic models for metanil yellow sorption onto nanosorbent

Parameters	Models & Equations	Initial concentration (mg/L)		
		20	40	60
q_e (Experimental)		7.12	8.17	10.75
k_1 (min^{-1})	Pseudo-first-order	0.022	0.010	0.003
q_e	$q_t = q_e[1 - exp(-k_1 t)]$	3.152	4.163	6.265
R^2		0.857	0.872	0.884
SE		0.419	0.367	0.328
SSE		1.369	0.869	0.512
q_e(mg/g)	Pseudo-second-order	7.74	8.65	11.12
k_2 (g/mg/min)	$q_t = \frac{(k_2 q_e^2 t)}{(1 + k_2 q_e t)}$	1.56×10^{-3}	1.38×10^{-3}	1.25×10^{-3}
h (mg/g/min)		0.094	0.103	0.154
k_2 q_e(min^{-1})	$h = k_2 q_e^2$	0.012	0.012	0.014
R^2		0.992	0.995	0.998
SE		0.043	0.041	0.041
SSE		0.017	0.014	0.011
S (min^{-1})	Ion-Exchange	0.024	0.015	0.005
R^2	$F = \frac{q_t}{q_e}$	0.832	0.814	0.906
SE		0.181	1.326	0.068
SSE	$B_t = -0.4977 - \ln(1 - F)$	0.326	5.259	0.004
A	$B_t = St$	0.608	0.426	0.367
k_0	Bangham diffusion	0.006	0.005	0.004
R^2	$log\left[log\left(\frac{C_o}{(C_o - q_t m)}\right)\right] = log\left(\frac{k_0 m}{2.303} V\right) + A \log t$	0.615	0.689	0.725
SE		0.254	0.216	0.174
SSE		0.720	0.462	0.231
k_i (mg/g/$min^{-0.5}$)	Intraparticle diffusion	0.131	0.126	0.134
C	$q_t = k_i t^{0.5} + C$	5.443	6.965	9.584
R^2		0.913	0.921	0.983
SE		0.063	0.041	0.027
SSE		0.004	0.002	0.001
Initial biosorption factor, R_i	$R_i = \frac{\left(k_i t_{ref}^{0.5}\right)}{q_{ref}}$	0.721	0.784	0.845
C/q_{ref}	$C/q_{ref} = 1 - R_i$	0.279	0.216	0.145
D_f(cm^2/s)	Film diffusion	2.25 X 10^{-8}	1.61 X 10^{-8}	1.25 X 10^{-8}
R^2	$\frac{q_t}{q_e} = 6\left(\frac{D_f}{\pi r^2}\right)^{0.5} t^{0.5}$	0.815	0.873	0.902
SE		0.372	0.312	0.302
SSE		0.918	0.901	0.793
D_p(cm^2/s)	Pore diffusion	1.82 X 10^{-9}	1.56 X 10^{-9}	1.34 X 10^{-9}
R^2	$B = \pi \frac{D_p}{r^2}$	0.911	0.917	0.924
SE		0.324	0.272	0.244
SSE		1.016	0.915	0.898

equilibrium capacity and deviated from linearity after 3 min, indicating limited applicability beyond 30 min. This deviation is attributed to the slower biosorption occurring within the pores of the biochar, which follows the rapid initial dye uptake on its surface[19]. This gradual intraparticle diffusion continues, causing slow changes in the equilibrium state of biosorption. As a result, the pseudo-first-order kinetic model is typically applicable only during the initial 30 min of the biosorption process. Since the Yang and Al-Duri modified pseudo-first-order formulation retains the same nonlinear form as the standard PFO while enforcing consistent parameter units, only a single nonlinear PFO fit was retained to avoid redundant parameter estimation[3]. The predicted data from the modified pseudo-first order model were more structured than the pseudo-first order model. The values of equilibrium capacity (q_e) and R^2 were also

higher than pseudo-first order model. Though the modified pseudo-first order equation could reduce the deviation of the experimental points, it could not describe the experimental data.The pseudo-second order model provided a much better fit (R^2 = 0.992–0.998), with predicted equilibrium capacities closely matching experimental values (Table 1, Fig. 2). The model suggests that adsorption kinetics are consistent with surface-controlled interactions rather than purely physical diffusion. Notably, the rate constant (k_2) decreased with higher initial dye concentration, while the initial sorption rate (h) increased, likely due to enhanced driving force[20].

To further examine the early-stage adsorption behaviour, the Boyd model was applied[21]. Reasonable linearity was observed during the initial 30 min (R^2 = 0.815–0.906), indicating that external mass transfer or ion-exchange effects may influence the initial uptake of metanil yellow onto the nanosorbent. The Boyd constant (S) represents the apparent rate of fractional uptake during this stage and serves as a diagnostic parameter rather than a mechanistic rate constant. Although the magnitude of S was comparable to kinetic constants obtained from pseudo-first-order analysis, such numerical similarity does not imply equivalence of adsorption mechanisms. Deviation from linearity at longer contact times suggests that ion-exchange is not the sole rate-controlling process and that additional transport or surface interaction steps govern the later stages of adsorption. Similar early-stage Boyd behaviour has been reported for the biosorption of Pb(II) onto mansonia sawdust[22] and safranin O onto macro fungus[23].

Since the dye uptake onto nanosorbent slowed down during the later stages of the biosorption, the Bangham's equation was applied to the kinetic data[24]. The Bangham model revealed that pore diffusion was not the sole rate-limiting step, as indicated by non-linear plots. Intraparticle diffusion analysis (q_t vs $t^{1/2}$, Fig. 3) showed a three-stage process: (i) boundary layer diffusion within 20 min, (ii) intraparticle diffusion through nanosorbent pores over the next 60 min, and (iii) equilibrium stage (Table 1) [25,26]. Increasing dye concentrations enhanced boundary layer thickness (C) and intraparticle diffusion rate constants (k_{ip}), suggesting improved diffusion and biosorption due to stronger concentration gradients[27]. The initial biosorption behaviour was determined based on the following equations[27].

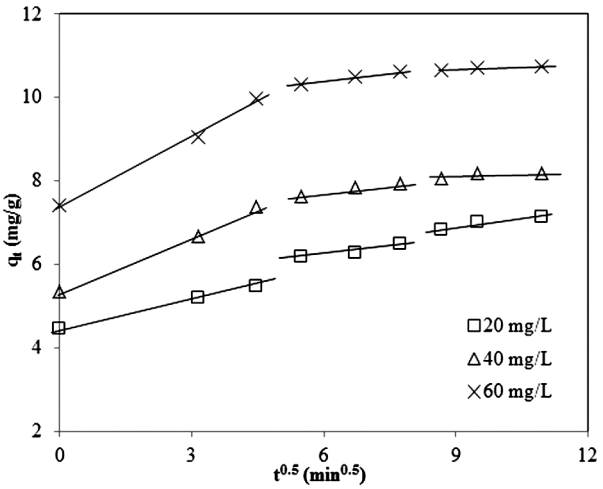

Fig. 3 — The intraparticle diffusion plot for sorption of metanil yellow ontonanosorbent (pH: 4.0, biosorbent dose: 2.0 g/L, temperature: 25°C, agitating rate: 140 rpm)

The Weber-Morris intraparticle diffusion rate equation ($q_t = k_i t^{0.5} + C$) can be written as:

$$q_{ref} = k_i \, t_{ref}^{0.5} + C \qquad \ldots (2)$$

Where t_{ref} is the longest time in the biosorption process and q_{ref} is the solid phase concentration at time t = t_{ref} for a biosorption system. Subtract Eq. (2) from intraparticle diffusion rate equation and after rearrangement will result in Eq. (3)

$$\left(\frac{q_t}{q_{ref}}\right) = 1 - R_i\left[1 - \left(\frac{t}{t_{ref}}\right)^{0.5}\right] \qquad \ldots (3)$$

Where $R_i = (k_i t_{ref}^{0.5} / q_{ref})$, defined as the initial biosorption factor and the characteristics curve based on the intraparticle diffusion model can be defined from Eq. (3). R_i is expressed as

$$R_i = \frac{q_{ref} - C}{q_{ref}} = 1 - \left(\frac{C}{q_{ref}}\right) \qquad \ldots (4)$$

Thus, Eq. (4) indicates that R_i can be represented in terms of the ratio of the initial biosorption amount (C) to the final biosorption amount (q_{ref}). The R_i and C/q_{ref} value were calculated for the effect of initial concentration of metanil yellow onto nanosorbent (Table 1). The values of R_i were ranged from 0.845 to 0.721 and while C/q_{ref} varied between 0.155 and 0.279. These values fell within zone 2 in Table 2, which demonstrated that initial biosorption is

Table 2 — Initial adsorption factor (R_i) and kinetic behaviour based on intraparticle diffusion

Ri	Initial point of kinetic curve (C/q_{ref})	Initial biosorption behaviour	Zone
R_i= 1	C/q_{ref} = 0	No initial biosorption	0
1 >R_i> 0.	9 0 <C/q_{ref}< 0.1	Weakly initial biosorption	1
0.9 >R_i> 0.5	0.1 <C/q_{ref}< 0.5	Intermediate initial biosorption	2
0.5 >R_i> 0.1	0.5 <C/q_{ref}< 0.9	Strong initial biosorption	3
R_i<0.1	C/q_{ref}> 0.9	Approaching complete initial biosorption	4

intermediate during the biosorption. The initial biosorption became weaker with increase in initial concentration from 20 to 60 mg/L, and almost insignificant as seen from the values of R_i approaching towards 0.9, while C/q_{ref} values just above 0.1, indicated the importance of intraparticle diffusion[22].

Both film diffusion and diffusion within the biosorbent control the intraparticle diffusion process. Assuming biosorbent particle to be of spherical shape with radius '*r*' and diffusion follows Fick's law, the relationship between uptake and time[28].

$$\frac{q_t}{q_e} = 6\left(\frac{D_t}{r^2}\right)\left[\pi^{-0.5} + 2\sum\sum_{n=1}^{\infty} ierfc\frac{nr}{Dt^{0.5}}\right] - 3\frac{Dt}{r^2} \quad \ldots(5)$$

At small times, D is replaced by D_f and Eq. (5) reduces to:

$$\frac{q_t}{q_e} = 6\left(\frac{D_f}{\pi r^2}\right)^{0.5} t^{0.5} \quad \ldots (6)$$

The fractional uptake of the dye was found to vary as a function of the square root of time ($t^{0.5}$), exhibiting a trend similar to that observed in the intraparticle diffusion plots. Film diffusion coefficients (D_f) corresponding to different dye concentrations were calculated from the plots of q_t/q_e versus $t^{0.5}$ as presented in Table 1. For moderate to longer time intervals, the relationship between dye uptake and time can be described by the diffusion equation:

$$\frac{q_t}{q_e} = 1 - \frac{6}{\pi^2}\left[\sum_{n=1}^{\infty}\frac{1}{n^2}\exp\left(\frac{-Dn^2\pi^2 t}{r^2}\right)\right] \quad \ldots (7)$$

As t tends to large times, Eq. (7) can be written in the form.

$$1 - \frac{q_t}{q_e} = \frac{6}{\pi^2}\exp(-Bt) \quad \ldots (8)$$

Where, $B = (D_2\Pi^2/r^2)$, Eq. (8) can be rearranged as:

$$Bt = -0.4997 - \ln\left(1 - \frac{q_t}{q_e}\right) \quad \ldots (9)$$

Eq. (9) was employed to calculate the *Bt* values for different initial dye concentrations. These *Bt* values were then plotted against time to determine whether external mass transfer or intraparticle diffusion was the dominant mass-transfer contribution in the biosorption process[21]. The resulting plots were linear during the initial phase but did not pass through the origin, suggesting that external mass transfer governed the initial rate of biosorption. Notably, as the initial dye concentration increased, the intercept moved closer to zero, indicating a greater contribution of external mass transfer. The slopes (*B*) of the *Bt* versus time plots at various initial concentrations were used to compute the pore diffusion coefficient (*Dp*) using the following equation:

$$B = \pi^2\frac{D_p}{r^2} \quad \ldots (10)$$

Both the film diffusion (D_f) and pore diffusion (D_p) coefficients decreased with increase in initial dye concentration due to decrease in available open sites to biosorption (Table 1). The results also illustrated that the pore diffusion is faster than the film diffusion. Similar results have been reported for adsorption of malachite green onto activated carbon[29].

Although multiple kinetic and diffusion models were applied in this study, their use was intended to provide complementary, rather than redundant, insight into the adsorption process. Among the evaluated kinetic models, the pseudo-second-order model most accurately described the experimental data and was

Table 3 — Various isotherms for metanil yellow sorption on nanosorbent and their parameters

Langmuir	*Freundlich*	Dubinin-Radushkevich (D-R)	*Temkin*	*Sips*
$q_e = \frac{q_m K_L C_e}{1 + K_L C_e}$	$q_e = K_F C_e^{\frac{1}{n}}$	$q_e = q_m \exp(-Be^2)$ $e = RT \ln\left(1 + \frac{1}{C_e}\right)$ $E = \frac{1}{\sqrt{2B}}$	$\theta = \frac{RT}{b_T} ln(K_T C_e)$	$q_e = \frac{K_S C_e^{\gamma}}{1 + a_S C_e^{\gamma}}$
q_m (mg/g) = 24.3	K_F(L/g) = 0.0285	q_m (mg/g) =87.41	b_T= 0.354	K_S (mg/g) =23.57
K_L(L/mg) = 0.971	n =0.768	B (mol^2 /kJ^2)= 0.002	K_T(L/mg)= 0.148	a_S(L/mg)= 0.479
R^2=0.995	R^2=0.865	E (kJ/mol) = 15.43	R^2=0.884	γ=0.927
SE =0.022	SE =0.954	R^2=0.942	SE =2.102	R^2=0.997
SSE=0. 004	SSE=4.424	SE =0.534	SSE=9.242	SE =0.014
		SSE=2.145		SSE=0.002

therefore treated as the primary kinetic framework. The remaining models, including pseudo-first-order, Boyd, Bangham, and diffusion-based analyses, were applied as diagnostic tools to examine early-stage mass transfer behaviour and transport limitations. These models were not used to independently assign rate-controlling mechanisms but to qualitatively support the observed transition from rapid surface uptake to slower intraparticle diffusion-controlled stages.

Biosorption isotherms

Biosorption isotherms illustrate the interaction between the biosorbent and the adsorbate and play a crucial role in optimizing the design and efficiency of biosorption systems. In this study, commonly applied isotherm models—including Langmuir, Freundlich, Dubinin–Radushkevich (D–R), Temkin, and Sips—were employed to analyse the adsorption of metanil yellow onto the nanosorbent. The model constants, statistical parameters, and corresponding equations are presented in Table 3.

The equilibrium data indicated that the adsorption process predominantly involves monolayer coverage of metanil yellow on the nanosorbent surface. This conclusion is supported by the strong fit to the Langmuir isotherm model (R^2 = 0.995) and the significant deviation observed with the Freundlich model, which assumes multilayer adsorption (Fig. 4). Additionally, the standard error (SE) and sum of squared errors (SSE) were lower for the Langmuir model compared to the Freundlich, further confirming the appropriateness of the Langmuir fit. These findings suggest that the biosorbent surface behaves as relatively homogeneous with respect to the dominant adsorption sites under the studied conditions. The maximum adsorption capacity

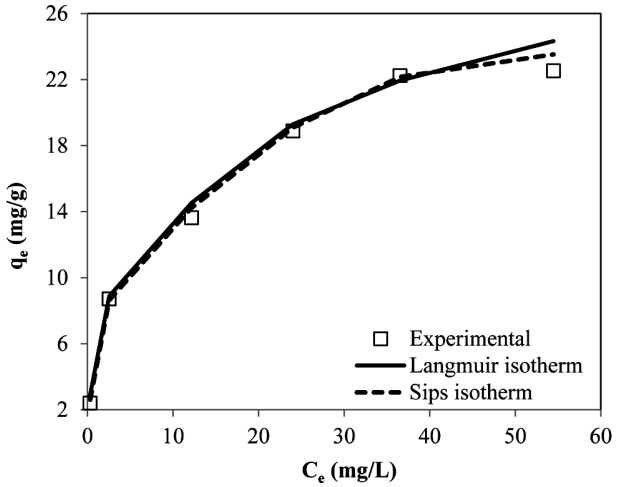

Fig. 4 — Biosorption isotherms of metanil yellow by nanosorbent (pH: 4.0, biosorbent dose: 2.0 g/ L, temperature: 25°C, agitating rate: 140 rpm, contact time: 300 min)

estimated from the Langmuir isotherm was 24.3 mg/g and the separation factor, R_L lies between 0 and 1, which confirmed that the removal of metanil yellow by nanosorbent is favourable[30]. The Langmuir isotherm model has also been found to suit the sorption of metanil yellow on to other sorbents such as Mg-Fe-NO_3 layered double hydroxide[14], chemically cross-linked chitosan beads[16] and fly ash/activated carbon[15]. The n values of Freundlich equation were greater than 2 indicating that the metanil yellow was favourably adsorbed by the nanosorbent[31]. This is in complete concurrence with the findings related to R_L value in case of the Langmuir isotherm.

Table 4 compares the experimental sorption capacities of metanil yellow for different sorbents reported in the literature with those obtained in the present study under aqueous conditions. The dye

Table 4 — Various adsorbents used for sorption of metanil yellow

Adsorbent	pH	Sorption capacity (mg/g)/sorption efficiency (%)	Reference
The nanoparticles of Mg-Fe-LDH-NO_3	9.5	42.72/85.44	[14]
Mehagani sawdust	-	132.5	[15]
Ionically and chemically cross-linked chitosan beads	4.0	1334	[16]
Sawdust	3.0	183.8	[19]
Mesoporous aluminophosphate	-	75	[32]
Amino functionalize dgraphenes (NH_2-G)	7.0	71.62	[33]
Rice husk		86.9	[38]
Bacillus sp. strain AK1 and *Lysinibacillus* sp. strain AK2	7.2	100	[39]
H_3PO_4 activated cassava peels carbon	-	19.22/12.04	[40]
Polyaniline-bentonite composite	-	188	[41]
Hen egg membrane	3.0	129.88	[42]
Carbonized pistachio shell magnetic nanoparticles	2.0	94%	[43]
Nanosorbent derived from *Jatropha* oil cake	4.0	24.3	Present study

sorption capacity of nanosorbent was found to be higher and comparable to other adsorbents except chemically cross-linked chitosan beads[16], mesoporous alumino phosphates[32], graphene[33] and saw dust[19]. Though the maximum biosorption capacity is based on batch experimental data, the low-cost nanosorbent shows potential for the removal of metanil yellow from contaminated wastewater.

Although the maximum adsorption capacity obtained in this study is modest compared to some high-capacity adsorbents reported in the literature (Table 4), the practical relevance of the present nanosorbent lies beyond adsorption capacity alone. The material is derived from an abundant agro-industrial residue, requires minimal processing, and exhibits favourable mass-transfer behaviour. In addition, its regeneration efficiency and reuse potential, discussed in a later section, further support its suitability for practical wastewater treatment applications where cost, material availability, and operational sustainability are critical considerations.

The D–R and Temkin isotherms also provided a reasonable fit to the experimental data, as indicated by their relatively high R^2 values and low SE and SSE values. In contrast, the Freundlich model showed poor agreement, with the lowest R^2 and the highest SE and SSE values, indicating significant deviation from the observed data. The D–R isotherm parameter, mean free energy (E), offers insight into the nature of the sorption mechanism—whether it is physical adsorption or chemical ion exchange. In this study, the calculated E value was 15.2 kJ/mol, suggested that the adsorption of metanil yellow onto the nanosorbent surface is likely governed by an ion-exchange mechanism[34].

A comparison between the experimental data and the values predicted by the studied isotherm models revealed that the Sips model[35] provided the most accurate fit, exhibiting the highest correlation coefficient (R^2 = 0.997) along with the lowest standard error (SE = 0.014) and sum of squared errors (SSE = 0.002) (Fig. 4). The Sips model exponent (γ), which reflects surface heterogeneity, deviates further from unity in highly heterogeneous systems[36]. In this study, the γ value was 0.927, suggesting that the sorption behaviour of metanil yellow aligns more closely with the Langmuir model than the Freundlich model. Furthermore, the maximum sorption capacity (q_m) predicted by the Sips model was consistent with the experimental data and lower than that estimated by the Langmuir model. Therefore, among the evaluated isotherms, the Sips model most accurately describes the experimental results.

Characterization of the nanosorbent

The TEM analysis (Fig. 5) showed that the nanosorbent consisted of primary particles in the nanoscale range (60–80 nm), which were partially aggregated into larger clusters. Such aggregation is typical for biochar-derived nanomaterials due to surface functional groups and interparticle interactions, and does not negate the presence of

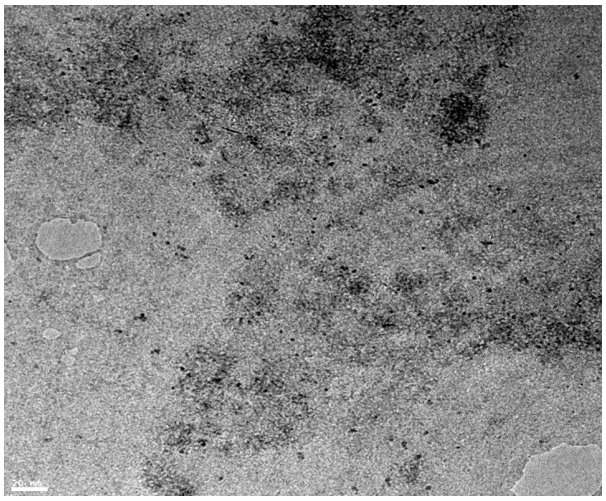

Fig. 5 — TEM image of nanosorbent prepared from *Jatropha* oil cake

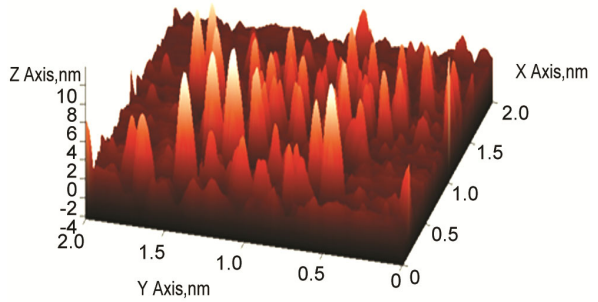

Fig. 6 — AFM image of nanosorbent prepared from *Jatropha* oil cake

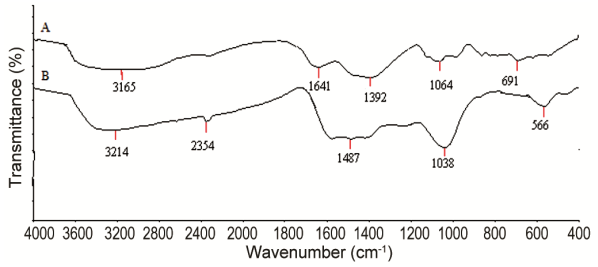

Fig. 7 — FT-IR spectra of (a) virgin nanosorbent and (b) metanil yellow adsorbed nanosorbent

nanoscale structural features[37]. AFM imaging (Fig. 6) revealed crystalline structures with laterally aggregated nanoparticles averaging 50 nm in diameter.In this study, the term "nanobiomaterial" refers to a bio-derived adsorbent composed of nanoscale primary particles, rather than a fully dispersed nanoparticle system. FTIR analysis (Fig. 7) was conducted to identify the functional groups involved in metanil yellow biosorption. Comparing spectra before and after biosorption revealed shifts in several characteristic peaks (≥4 cm^{-1}), indicating changes in surface chemistry. Notably, the –OH band shifted from 3165 to 3214 cm^{-1}, indicating the involvement of hydroxyl groups in dye interaction[29]. Shifts observed in C–O and C–N stretching vibrations further suggest participation of oxygen- and nitrogen-containing functional groups during adsorption[17]. Taken together, the FTIR results, when interpreted alongside pH-dependent adsorption behaviour and pH_{pzc} analysis, indicate that ion-exchange and surface complexation contribute to metanil yellow uptake, without implying a single dominant mechanism.

Desorption and regeneration

Desorption of metanil yellow from the loaded nanosorbent is important for disposal and reuse of the dye as well as applications of nanosorbent in industrial practice. All the reagents showed good desorption efficiency and the percentage of metanil yellow desorbed from 0.1 g of the used nanosorbent were 98.4, 97.8, 97.4, 93.2 and 91 for acetone, NaOH, HCl, EDTA, and acetic acid, respectively. Acetone was further employed for five cycles of adsorption-desorption and the results showed that the desorbing efficiencies were 98.4, 97.5, 96.9, 96.6 and 96.3 for first, second, third, fourth and fifth cycle, respectively. High desorption efficiency observed with acetone and HCl supports the contribution of ion-exchange interactions during adsorption[17]. Similarly, the nanosorbent demonstrated excellent reusability, retaining its sorption capacity with only a minimal reduction of approximately 6–8% after five adsorption–desorption cycles. Notably, no material loss was observed during these cycles, underscoring the nanosorbent's potential for practical and scalable industrial applications. Additionally, metanil yellow-loaded nanosorbent could potentially be immobilized in construction materials or fuel briquettes, providing a possible route for safe containment of the dye.

From a practical application perspective, considerations beyond batch performance are important. Although experiments were conducted using synthetic dye solutions, the broad pH tolerance and rapid uptake kinetics suggest that the nanosorbent may remain effective in complex wastewater systems with variable chemistry. Acetone proved to be an efficient desorbing agent, indicating strong regeneration potential, although solvent consumption and recovery would require optimization at larger scales. The use of an abundant agro-industrial residue and minimal processing requirements partially offset the moderate adsorption capacity in terms of cost and sustainability. While batch studies provide mechanistic insight, future evaluation in continuous or

fixed-bed systems is needed to assess operational feasibility under realistic conditions.

Conclusion

A nanosorbent derived from *Jatropha* oil cake was investigated as a cost-effective biosorbent for the removal of metanil yellow dye from aqueous solutions, focusing on sorption kinetics, isotherms, and desorption behaviour. The dye adsorption process at varying initial concentrations followed a pseudo-second-order kinetic model, indicating surface-controlled adsorption behaviour. The initial biosorption factor (*Ri*) indicated a moderate initial uptake. Mass transfer and intraparticle diffusion were identified as important contributors to the overall rate of the biosorption process. FTIR analysis before and after dye adsorption, together with pH-dependent sorption trends and pH_{pzc} considerations, suggests that ion-exchange and surface complexation contribute to the interaction between metanil yellow and the biosorbent. Equilibrium adsorption data were best described by the Sips isotherm model, followed by the Langmuir model. Effective desorption of metanil yellow was achieved using acetone and HCl. This study highlights the potential of *Jatropha* oil cake-based nanosorbent as a sustainable and low-cost material for dye removal from wastewater. The approach not only addresses environmental challenges but also adds value to a by-product of biodiesel production. Understanding the adsorption kinetics and equilibrium behaviour paves way for optimizing the use of *Jatropha*-based nanomaterials in large-scale water treatment applications.

Conflict of interest

The authors declare that they have no conflict of interest.

Acknowledgements

The authors are thankful to Directors of CSIR-CSMCRI, CSIR-CLRI and CSIR-NEERI for their constant encouragement and support.

References

1 Ahmed M J & Dhedan S K, Equilibrium isotherms and kinetics modeling of methylene blue adsorption on agricultural wastes-based activated carbons, *Fluid Phase Equilib*, 317 (2012) 9.
2 Cicek F, Ozer D, Ozer A & Ozer A, Low cost removal of reactive dyes using wheat bran, *J Hazard Mater*, 146 (2007) 408.
3 Yang X & Al-Duri B, Kinetic modeling of liquid-phase adsorption of reactive dyes on activated carbon, *J Colloid Interf Sci*, 287 (2005) 25.
4 Thirunavukkarasu A, Nithya R & Sivashankar R, Continuous fixed-bed biosorption process: A review, *Chem Eng J Adv*, 8 (2021) 100188.
5 Saha P D, Chowdhury S, Mondal M & Sinha K, Biosorption of direct red 28 (Congo Red) from aqueous solutions by eggshells: Batch and column studies, *Sep Sci Technol*, 47 (2012) 112.
6 Yakout S M, Monitoring the changes of chemical properties of rice straw-derived biochars modified by different oxidizing agents and their adsorptive performance for organics, *Bioremediat J*, 19 (2015) 171.
7 Muliadi F N A, Halmi M I E, Wahid S B A, Gani S S A, Mahmud K & Shukor M Y A, Immobilization of metanil yellow decolorizing mixed culture FN3 using gelling gum as matrix for bioremediation application, *Sustainability*, 13 (2020) 36.
8 Selvaraj V, Karthika T S, Mansiya C & Alagar M, An overview on recently developed techniques, mechanisms and intermediate involved in the advanced azo dye degradation for industrial applications, *J Mol Struct*, 1224 (2021) 129195.
9 Asgher M & Bhatti H N, Evaluation of thermodynamics and effect of chemical treatments on sorption potential of citrus waste biomass for removal of anionic dyes from aqueous solutions, *Ecol Eng*, 38 (2012) 79.
10 Gupta V K, Ali I, Suhas & Mohan D, Equilibrium uptake and sorption dynamics for the removal of a basic dye (basic red) using low-cost adsorbents, *J Colloid Interf Sci*, 265 (2003) 257.
11 Garg U, Kaur M P, Jawa G K, Sud D & Garg V K, Removal of cadmium (II) from aqueous solutions by adsorption on agricultural waste biomass, *J Hazard Mater*, 154 (2008) 1149.
12 Mansuri N, Mody K & Basha S, Biosorption of ammoniacal nitrogen from aqueous solutions with low-cost biomaterials: Kinetics and optimization of contact time, *Int J Environ Sci Technol*, 11 (2014) 1711.
13 Kurniawan A & Ismadji S, Potential utilization of *Jatropha curcas L*. press-cake residue as new precursor for activated carbon preparation: Application in methylene blue removal from aqueous solution, *J Taiwan Inst Chem Eng*, 42 (2011) 826.
14 Nejati K, Rezvani Z, Mansurfar M, Mirzaee A & Mahkam M, Adsorption of metanil yellow azoic dye from aqueous solution onto Mg-Fe-NO_3 layered double hydroxide, *Z Anorg Allg Chem*, 637 (2011) 1573.
15 Santra A K, Pal T K & Datta S, Removal of metanil yellow from its aqueous solution by fly ash and activated carbon produced from different sources, *Sep Sci Technol*, 43 (2008) 1434.
16 Chiou M S & Chuang G S, Competitive adsorption of dye metanil yellow and RB15 in acid solutions on chemically cross-linked chitosan beads, *Chemosphere*, 62 (2006) 731.
17 Wan N W S & Hanafiah M A K M, Biosorption of copper ions from dilute aqueous solutions on base treated rubber (*Heveabrasiliensis*) leaves powder: kinetics, isotherm, and biosorption mechanisms, *J Environ Sci*, 20 (2008) 1168.
18 Ho Y S, Citation review of Lagergren kinetic rate equation on adsorption reactions, *Scientometrics*, 59 (2004) 171.

19 Ozacar M & Sengil I A, Adsorption of metal complex dyes from aqueous solutions by pine sawdust, *Bioresour Technol*, 96 (2005) 791.

20 Hameed B H, Tan I A W & Ahmad A L, Adsorption isotherm, kinetic modeling and mechanism of 2,4,6-trichlorophenol on coconut husk-based activated carbon, *Chem Eng J*, 144 (2008) 235.

21 Boyd G E, Schubert J & Adamson A W, The exchange adsorption of ions from aqueous solutions by organic zeolites. I. Ion-exchange equilibria, *J Am Chem Soc*, 69 (1947) 2818.

22 Ofomaja A E, Intraparticle diffusion process for lead (II) biosorption onto mansonia wood sawdust, *Bioresour Technol*, 101 (2010) 5868.

23 Maurya N S & Mittal A K, Removal mechanism of cationic dye (Safranin O) from the aqueous phase by dead macro fungus biosorbent, *Water Sci Technol*, 68 (2013) 1048.

24 Aharoni C, Sideman S & Hoffer E, Adsorption of phosphate ions by collodion-coated alumina, *J Chem Technol Biotechnol*, 29 (1979) 404.

25 Feng Y, Dionysiou D D, Wu Y, Zhou H, Xue L, He S & Yang L, Adsorption of dyestuff from aqueous solutions through oxalic acid-modified swede rape straw: adsorption process and disposal methodology of depleted bioadsorbents, *Bioresour Technol*, 138 (2013) 191.

26 Mittal A, Thakur V & Gajbe V, Evaluation of adsorption characteristics of an anionic azo dye Brilliant Yellow onto hen feathers in aqueous solutions, *Environ Sci Pollut Res*, 19 (2012) 2438.

27 Wu F C, Tseng R L, Huang S C & Juang R S, Characteristics of pseudo-second-order kinetic model for liquid-phase adsorption: A mini-review, *Chem Eng J*, 151 (2009) 1.

28 Crank J, The mathematics of diffusion, 2nd Edn, Oxford University Press, Oxford (1979).

29 Onal Y, Akmil-Basar C & Sarici-Ozdemir C, Investigation kinetics mechanisms of adsorption malachite green onto activated carbon, *J Hazard Mater*, 146 (2007) 194.

30 Hall K R, Eagleton L C, Acrivos A & Vermeulen T, Pore-and solid-diffusion kinetics in fixed-bed adsorption under constant-pattern conditions, *Ind Eng Chem Fundam*, 5 (1966) 212.

31 Treybal R E, Mass-transfer operations, 3rd Edn (McGraw-Hill Book Company, New York), 1980.

32 Muthuraja K & Kannan C, Kinetic and isotherm studies of removal of metanil yellow dye on mesoporous aluminophosphate molecular sieves, *Chem Sci Trans*, 2 (2013) S195.

33 Guo X, Wei Q, Du B, Zhang Y, Xin X, Yan L & Yu H, Removal of Metanil Yellow from water environment by amino functionalized graphenes (NH2-G): Influence of surface chemistry of NH2-G, *Appl Surf Sci*, 284 (2013) 862.

34 Onyango M S, Kojima Y, Aoyi O, Bernardo E C & Matsuda H, Adsorption equilibrium modeling and solution chemistry dependence of fluoride removal from water by trivalent-cation-exchanged zeolite F-9, *J Colloid Interf Sci*, 279 (2004) 341.

35 Sips R, On the structure of a catalyst surface, *J Chem Phys*, 16 (1948) 490.

36 Ko D C K, Porter J F & McKay G, Optimised correlations for the fixed-bed adsorption of metal ions on bone char, *Chem Eng Sci*, 55 (2000) 5819.

37 Bantz C, Koshkina O, Lang T, Galla H J, Kirkpatrick C J, Stauber R H & Maskos M, The surface properties of nanoparticles determine the agglomeration state and the size of the particles under physiological conditions, *Beilstein J Nanotechnol*, 5 (2014) 1774.

38 Malik P K, Use of activated carbons prepared from sawdust and rice-husk for adsorption of acid dyes: A case study of Acid Yellow 36, *Dyes Pigm*, 56 (2003) 239.

39 Anjaneya O, Souche S Y, Santoshkumar M & Karegoudar T B, Decolorization of sulfonated azo dye Metanil Yellow by newly isolated bacterial strains: *Bacillus sp.* strain AK1 and *Lysinibacillus sp.* strain AK2, *J Hazard Mater*, 190 (2011) 351.

40 Isiuku B O, Horsfall M J J & Spiff A I, Adsorption of metanil yellow on chemically-activated carbon in a packed-bed column: effect of activation reagent, *ARPN J Eng Appl Sci*, 8 (2013) 282.

41 Meng F, Wang L, Pei M, Guo W & Liu G, Adsorption of metanil yellow from aqueous solution using polyaniline-bentonite composite, *Colloid Polym Sci*, 295 (2017) 1165.

42 Isiuku B O & Ibe F C, Removal of metanil yellow by batch biosorption from aqueous phase on egg membrane: equilibrium and isotherm studies, *Anal Methods Environ Chem J*, 2 (2019) 15.

43 Adnan, Omer M, Khan B, Khan I, Alamzeb M, Zada F M, Ullah I, Shah R, Alqarni M & Simal-Gandara J, Equilibrium, kinetic and thermodynamic studies for the adsorption of metanil yellow using carbonized pistachio shell-magnetic nanoparticles, *Water*, 14 (2022) 4139.